Density Functional Theory Study of the Structure and Energetics of Negatively Charged Oligopyrroles

YAFEI DAI,[1] SUGATA CHOWDHURY,[1] ESTELA BLAISTEN-BAROJAS[1,2]

[1]*Computational Materials Science Center, George Mason University, MS 6A2, Fairfaax, VA 22030*

[2]*Department of Computational and Data Sciences, George Mason University, MS 6A2, Fairfax, VA 22030*

Received 6 December 2009; accepted 10 February 2010
Published online 29 June 2010 in Wiley Online Library (wileyonlinelibrary.com).
DOI 10.1002/qua.22659

ABSTRACT: First-principles calculations are used to investigate the electronic properties of negatively charged *n*-pyrrole oligomers with $n = 2$–18. Chains of neutral oligomers are bent, whereas the negatively charged oligomers become almost planar due to accumulation of negative charge at the end monomers. Isomers of short oligomers ($n < 6$) display negative electron affinity although the corresponding anions are energetically stable. For longer oligomers with $n \geq 6$, the electron affinity is small and positive, slowly increasing with oligopyrrole length. Doping of 12-pyrrole with lithium atoms shows that negative oxidation states are possible due to electron transfer from dopant to oligomer at locations close to dopant. These 12-pyrrole regions support extra negative charge and exhibit a local structural change from benzenoid to quinoid structure in the C—C backbone conjugation. Comparison between neutral and doped polypyrrole (PPy) indicates that doped polymers displays a substantial depletion of the band gap energy and the appearance of dopant-based bands in the gap for a 50% per monomer doping level. It is predicted that Li-doped PPy is not metallic. ©2010 Wiley Periodicals, Inc. Int J Quantum Chem 111: 2295–2305, 2011

Key words: oligopyrrole; polypyrrole; density functional theory; electron affinity; *n*-doping conducting polymers

1. Introduction

Since the discovery of polypyrrole (PPy) almost 50 years ago [1, 2], a myriad of publications are now available, more than 800 this past year alone according to Web of Science. PPy is a prototype conducting polymer [3] that displays unique mechanical, optical, electrical, and biocompatible properties. However, much about the physical properties and structural characteristics of PPy are still not well understood, with data that is often contradictory. With the advent of nanomaterials, today PPy is used as a component

Correspondence to: E. Blaisten-Barojas; e-mail: blaisten@gmu.edu

Contract grant sponsor: National Science Foundation.
Contract grant number: CHE0626111.

© 2010 Wiley Periodicals, Inc.

at the nanoscale in a variety of sensors, fibers, and coated foams among other nanostructures [4, 5]. For example, when shaped as a conduit, PPy has been proven effective for biomaterials modification and regeneration of damaged nerves [6, 7]. Polymerization occurs either electrochemically or chemically with dopant anions that remain embedded into the polymeric matrix. This constitutes the oxidized phase of PPy that displays conduction and possesses quinoid structure. Therefore, most commonly oxidized PPy is a polycationic conductor that synthesizes forming thin or thick films. A wide variety of electronegative dopants have been used, such as chloride ions, polystyrene sulfonate, molecular and polymeric anions, buffer salts [8–10], and several biologically active anions [7, 11]. Oxidation properties are crucial for affinity binding of peptides for chloride-doped PPy [12]. By reduction, the electrical conduction property is lost and the structure of the conjugated chain becomes benzenoid. However, the polymeric PPy matrix is difficult to be fully reduced, it is not crystalline, and displays regions of stacked chains [13]. Electrochemical switching from oxidized to reduced phases of PPy produces up to 30% change in the sample volume. This actuation property is exploited for artificial muscles [9, 10].

Oxidation by electronegative dopants that gain electrons from the polymer is equivalent to p-doping and is feasible because of the low work function of PPy. A different oxidation mechanism occurs when electropositive dopants donate electrons to the polymer (n-doping) turning PPy into a polyanionic system. This oxidation mechanism is difficult to realize by electrochemical means. In fact, researchers assess that they did not obtain stable doped systems when electropositive atoms or molecules were used in the electrochemical process [13]. The often accepted reason for n-doping not being favored is the low electron affinity of PPy and its oligomers. Therefore, PPy negative oxidation states have been elusive to experimentalists. The purpose of this article is the investigation of the electron affinity of Py oligomers and determination of the changes in the polymer backbone structure when oligopyrroles are doped with lithium.

Over the years, a series of theoretical studies have provided different predictions for oligopyrroles. For example, changes in the UV and visible absorption spectra of neutral and cation oligopyrroles due to chlorine dopants have been put forward within hybrid density functional theory (DFT) and pseudopotentials [14]. This publication provides an extensive bibliography on previous electronic structure calculations. Contemporarily to Ref. 14, we published [15] a careful study of oligopyrroles electronic structure and structure optimization in their reduced and multiply oxidized phases with fluorine dopants within all-electron DFT approach (B3PW91). Here, we apply the same methodology as in our pervious study [15] for investigation of the electron affinity, structural effects of doping with lithium, and changes in the electronic structure of oligopyrroles and PPy. A clear difference emerges by comparing the new results of negative oxidation levels with those previously obtained for positive oxidation levels.

Electronic structure studies of negatively oxidized PPy and oligopyrroles are scarce. Early work was done with low-level electronic structure calculations. The pioneer HF calculations with STO-3G basis sets of Bredas et al. [16] of tetrapyrrole (4-Py) with and without Na dopants (n-type) demonstrated an almost complete electron transfer between the doping atoms and pyrrole (Py) rings. Although the small basis set was inadequate for an accurate electronic structure description, this work predicted that the dominant state for conduction was attained with two doping Na atoms located adjacent to each other on top of two contiguous Py rings (50% per monomer doping level). This is referred in the literature as bipolaron. Very recent DFT studies of lithium-doped polythiophene [17] reported positive energies of formation for 20–100% per monomer doping levels. This prediction indicates the need of supplying to the oligomer about 5 kcal/mol for each pair of Li dopants to attain a doped system, which suggests a negative electron affinity of the oligothiophenes. Negative electron affinities of oligopyrroles n-Py up to $n = 16$ were reported within a molecular fragment approach [18], thus, predicting unfavorable negative oxidation of oligopyrroles. In this article, we calculate electron affinities of n-Py up to $n = 18$ within our more advanced first principles methodology.

Because calculation of electron affinities requires basis sets with polarization and diffuse functions, one double-ζ and two triple-ζ basis sets are considered here. This article is organized as follows. Section 2 describes the computational details for obtaining the electronic structure. Section 3 investigates the structure, energetics, and vibrational analysis of neutral and anion

bipyrrole, tripyrrole, and tetrapyrrole possible isomers. Additionally, the isomerization reactions in 3-Py and 4-Py anions from *anti-gauche* to *syn-gauche* structures are discussed in this section. Energetics and electron affinities of *n*-Py neutral and anion oligomers with $n \geq 6$ are reported in Section 4. This section contains a study of the charge distribution and structure and of lithium-doped 12-Py. Based on periodic boundary conditions (PBC), section 5 is dedicated to the study of the band structure of pristine and n-doped PPy by considering an infinite chain of a 4-Py motif decorated with two Li atoms. Section 6 concludes this article.

2. Methods

All-electron DFT within the Becke three-parameter hybrid approach [19] including local and nonlocal correlation functionals as implemented in Gaussian09 [20] is adopted throughout this study. The choice of the correlation functional is based on comparative results of Py structure using a variety of functionals: B3PW91 [21, 22], B3LYP [23, 24], B3BMK [25], and M06-HF [26]. Results closest to experiment [27] are obtained with B3PW91 reproducing the experimental C_{2v} planar structure of neutral Py monomer. The B3PW91 approach is then adopted, which additionally allow for comparison with our previous studies [15]. In the study of doped *n*-Py oligomers, where a considerable charge transfer takes place, comparison between results within B3PW91 and full exchange M06-HF approaches is reported.

Structures of oligomers are optimized using triple valence basis sets 6-311G, 6-311++G with diffuse functions and double valence basis sets 6-31+G (3d, 3p) with diffuse and polarization functions for all atoms. Comparison between the optimal calculated structure of neutral Py and experiment [27] indicates that these three basis sets yield comparable relative errors in the geometry: 0.38% with 6-311G, 0.42% with 6-311++G, and 0.37% with 6-31+G (3d,3p). The Py monomer has a strong dipole moment along the direction of the N—H bond (*Y*-axis) of 1.89 D with the 6-311++G basis sets (1.85 D with 6-31+G (3d,3p)). The quadrupole matrix is diagonal in a set of axis where the *X*-axis is perpendicular to the N—H bond and contained in the plane of the molecule and the *Z*-axis is perpendicular to the molecular plane passing through the center of the Py ring. The quadrupole matrix in this set of axis is diagonal with the XX, YY, ZZ matrix elements having values of −27.26, −24.11, −34.97 DÅ using 6-311++G and −27.55, −24.32, −34.33 DÅ using 6-31+G (3d,3p). These properties are in excellent agreement with our previous results using the 6-311G basis set without diffuse or polarization functions [15].

Geometry optimization for each *n*-Py oligomer is attained by minimizing the molecular electronic energy with respect to coordinates of all atoms in 3D using the Berny algorithm and redundant internal coordinates [28, 29]. Optimizations ensure accuracies of 10^{-4} for distances or angles and 10^{-8} Hartrees for energies. For *n*-Py optimized geometries, the vibrational analysis is routinely performed to attest for the existence of a minimum. For transition states (TS), the displacement of atoms corresponding to the vibrational mode associated with the imaginary frequency is checked to ensure that the TS geometry is attained. Furthermore, the intrinsic reaction coordinate method allows us to assess that the TS connects the two desired minima (two different isomers) along the potential energy surface [30, 31]. Solvent effects are included for the small oligomers with the polarized continuum model approach [32].

In forthcoming sections, binding energies *E* are reported with respect to the separated atoms energies: −13.7133 eV for H, −1027.4931 eV for C, and −1481.9450 eV for N with the 6-311G; −13.7156 eV for H, −1027.5601 eV for C, and −1482.0417 eV for N with the 6-311++G; −13.6642 eV for H, −1027.4197 eV for C, and −1482.0417 eV for N with the 6-31+G (3d,3p) basis sets.

The electron affinity EA is calculated as the difference between all-electron total energies:

$$\mathrm{EA} = E_{\mathrm{total}}(\mathrm{neutral}) - E_{\mathrm{total}}(\mathrm{anion}), \qquad (1)$$

where E_{total}(neutral) is the total energy of the optimized neutral oligomer and E_{total}(anion) is the total energy of the optimized singly negative-charged oligomer. Singly negative charged *n*-Py oligomers are referred to as anions in the following sections.

For PPy with PBC, the band structure is referred to the Fermi energy E_F. The value of E_F is obtained by solving a self consistent equation that equates the number of electrons *N* to the sum

TABLE I

Binding energies of *n*-Py and *n*-Py$^-$ stable isomers with *n* = 2, 3, 4. Energies are referred to the separated atoms energies given in Section 2.

			Neutral *E*/*n* (eV)				Anion *E*/*n* (eV)		
N	Isomer	State	6-311G	6-311++G	6-31+G(3d, 3p)	State	6-311G	6-311++G	6-31+G(3d,3p)
2	↑↓	C_2, ^1A	−53.4209	−53.1300	−54.9775	C_{2h}, ^2A_g	−52.6860	−52.9188	−54.6165
	↑↑	C_2, ^1A	−53.3599	−53.0954	−54.9399	C_{2v}, $^2A_1$	−52.6994	−52.9600	−54.6319
3	↑↓↑	C_1, ^1A	−52.6129	−52.3189	−54.1434	C_1, ^2A	−52.3243	−52.1983	−53.9450
	↑↑↓	C_1, ^1A	−52.5636	−52.2946	−54.1304	C_1, ^2A	−52.3362	−52.2122	−53.9570
	↑↑↑	C_1, ^1A	−52.5673	−52.2735	−54.1167	C_1, ^2A	−52.3448	−52.2743	−54.0018
4	↑↓↑↓	C_2, ^1A	−52.2097	−51.9145	−53.7274	C_1, ^2A	−51.0819	−51.8370	−53.6606
	↑↓↓↑	C_2, ^1A	−52.1968	−51.9007	−53.7040	C_1, ^2A	−51.0880	−51.8411	−53.6541
	↑↓↑↑	C_1, ^1A	−52.1922	−51.8974	−53.6994	C_1, ^2A	−51.0825	−51.8358	−53.6476
	↑↑↓↓	C_2, ^1A	−52.1793	−51.8844	−53.6851	C_1, ^2A	−51.0821	−51.8342	−53.6464
	↑↑↑↓	C_1, ^1A	−52.1784	−51.8827	−53.6837	C_1, ^2A	−51.0912	−51.8423	−53.6534
	↑↑↑↑	C_2, ^1A	−52.1582	−51.8630	−53.6733	C_1, ^2A	−51.0916	−51.9241	−53.6779

of electron occupation probabilities (Fermi functions) of eigenstates composing the bands:

$$N = \sum_{\alpha=1}^{n_{\text{band}}} \sum_{k=1}^{n_k} \frac{2}{1 + e^{\frac{(E_{\alpha,k} - E_F)}{K_B T}}} \tag{2}$$

where $n_{\text{band}} = 16$ is the number of bands considered in this work, $n_k = 81$ is the number of k-points in each band allowing up to 162 electrons per band, K_B is Boltzman's constant, $T = 600$ K is a broadening temperature and $N = 2n_k n_{\text{band}}$. Values of these parameters ensure accuracy of 0.01 eV in the determination of E_F.

3. Bipyrrole, Tripyrrole, and Tetrapyrrole Anions

The geometrical structure of bipyrrole, as well as that of longer oligomers, is modulated the most by the monomer rotational degree of freedom around the C—C bond joining contiguous monomers. Neutral bipyrrole (2-Py) has four stable isomers: two puckered structures *anti-gauche* and *syn-gauche*, and two planar structures *anti* and *syn* [15, 33]. These four neutral isomers are stable irrespective of the basis sets used. The *anti-gauche* isomer is the lowest in energy with a torsion angle around 150° followed by the *syn-gauche* isomer that lies a few hundredths eV above as reported in Table I and has a torsion angle around 50°. The cation 2-Py$^+$ displays two planar isomers: *anti* (C_{2h}) and *syn* (C_{2v}) and the transition between them is not thermally possible [15]. Our calculations of the anion 2-Py$^-$ demonstrate that the negatively charged molecule has also two possible planar isomers: *anti* (C_{2h}) and *syn* (C_{2v}). The lowest energy isomer of 2-Py$^-$ is the C_{2v} structure, whereas the C_{2h} structure is higher in energy as seen from values of the binding energies given in Table I. These electronic states are doublets, with very low spin contamination. Quartets states are several eVs less stable. With the triple-ζ basis sets the TS from the C_{2v} isomer to the C_{2h} isomer is 0.20 eV (0.26 eV with 6-31+G (3d, 3p)). This TS corresponds to a torsion barrier separating the two isomers. The high energy of this TS eliminates the possibility of thermally induced isomerization. Both anion isomers have electronic energies above their neutral counterparts. Consequently, the electron affinity EA is negative, as occurs in molecular anions where the extra electron is dipole-bound [34]. Values of EAs are reported in Table II. Performing one-point CCSD/6-31G* calculations of the optimized geometries of neutral and anion isomers confirms the above results; namely, the C_{2v} anion isomer is 0.13 eV more stable that the C_{2h} anion isomer and the EA is negative. Thus, we predict that 2-Py$^-$ will not be observed experimentally because if a fairly long lifetime of the anion is required for performing the measurement, electron recombination with the surroundings will occur before the measure takes place.

Combinations of *anti-gauche* with *syn-gauche* orientations of monomers in tripyrrole (3-Py$^-$)

TABLE II

Electron affinity of *n*-Py oligomers calculated from Eq. (1).

		EA (eV)	
n	Isomer	6-311++G	6-31+G (3d,3p)
2	↑↓	−0.4224	−1.1758
	↑↑	−0.2708	−1.2034
3	↑↓↑	−0.3618	−0.7944
	↑↑↓	−0.2472	−0.5739
	↑↑↑	0.0024	−0.1620
4	↑↓↑↓	−0.3100	−0.2672
	↑↓↓↑	−0.2384	−0.1996
	↑↓↑↑	−0.2464	−0.2072
	↑↑↓↓	−0.2008	−0.1548
	↑↑↑↓	−0.1616	−0.1212
	↑↑↑↑	0.2444	−0.0032
6		0.0432	0.0557
8		0.2396	0.2482
9		0.3087	0.3155
12		0.4634	0.4642
15		0.5709	0.5705
18		0.6475	0.6500

For $n > 4$ the most isomer reported is the most stable in which the *-anti-syn-* monomer orientation is repeated.

and tetrapyrrole (4-Py$^-$) give rise to three and six isomers, respectively. The three neutral isomers of 3-Py are shown in Figure 1(a). The ground states of these neutral isomers are singlet electronic states. Binding energies are reported in Table I, including comparison of results calculated with the three basis sets considered in this study. The vibrational analysis of isomers and their anion counterpart yields positive frequencies, indicating that the values reported in Table I correspond to minima of the potential energy surface. The 3-Py isomer of lowest energy, isomer I, has two 150° torsion angles (157° with 6-31+G (3d, 3p)) between monomer planes containing the N—H bond. Isomer III is the highest energy 3-Py isomer that has two 43° torsion angles between monomer planes (39° with 6-31+G (3d, 3p)). The two torsion angles in isomer II are 150° and 43° (157°, 39° with 6-31+G (3d, 3p)). Two TSs, TS_1 and TS_2, lie between these three isomers ground states at 0.11 eV and 0.17 eV (0.13, 0.15 eV using 6-31+G (3d, 3p)). The first transition structure has the third ring in isomer I rotated 90° while the second transition structure has the third ring of isomer II rotated 90°. Schematics of the potential energy along the isomerization path are depicted in Figure 1(b). Solvent effects, assuming a relative dielectric constant for water of 78.355, were considered. The overall effect of solvent is to stabilize the isomers and destabilize the TSs as indicated in parenthesis in Figure 1. Our transition energies are very close to the reported values of torsion barriers obtained by fixing the geometry of the rings and only relaxing both torsion angle and interring bond length [33, 35]. Geometry optimization of 3-Py$^-$ anion isomers yields almost planar structures in doublet states. Table I contains the binding energies of the three anion isomers corresponding to geometry-optimized structures. Isomer III, with the three N—H bonds pointing in the same side of the chain, is the most stable 3-Py$^-$. This anionic isomer has a marginal (almost zero) electron affinity as shown in Table II. Therefore, under favorable circumstances, a weak electron attachment to 3-Py isomer III may be observed because of a dipole binding mechanism [34]. However, the most stable neutral isomer I would need to overcome a 0.17 eV (0.15 eV with 6-31+G (3d, 3p)) isomerization barrier to transform into isomer III before an electron could be attached. Therefore, this process might be feasible at high temperatures only.

For tetrapyrrole, there are six isomers combining the *anti* and *syn* orientations of the N—H bonds. For simplicity, these isomers are represented with up/down arrows. States and binding energies are reported in Table I, which correspond to a full geometry optimization of each isomer and each anion. The vibrational analysis of all isomers and their anions yield positive frequencies indicating that energies reported correspond to minima of the electron energy surface. The 4-Py neutral isomer ↑↓↑↓ (torsion angles 150°, 151°, 150° with 6-311++G and 156°, 157°, 156° with 6-31+G (3d, 3p)) is the most stable and the isomer ↑↑↑↑ (41°, 33°, 41° with 6-311++G and 35°, 30°, 35° with 6-31+G (3d, 3p)) is the least stable. The other four neutral isomers are ordered in increasing energy order as ↑↓↓↑ (149°, 31°, 149° with 6-311++G and 155°, 27°, 155° with 6-31+G (3d, 3p)), ↑↓↑↑ (150°, 153°, 40° with 6-311++G and 156°, 158°, 36° with 6-31+G (3d, 3p)), ↑↑↓↓ (41°, 152°, 41° with 6-311++G and 36°, 157°, 36° with 6-31+G (3d, 3p)), and ↑↑↑↓ (40°, 35°, 149° with 6-311++G and 36°, 31°, 156° with 6-31+G (3d, 3p)).

The most stable 4-Py$^-$ anion is the ↑↑↑↑ isomer. This is an almost planar molecule with torsion angles 4°, 6°, 4° (3°, 4°, 3° with 6-31+G (3d, 3p)). This isomer displays a marginal almost zero

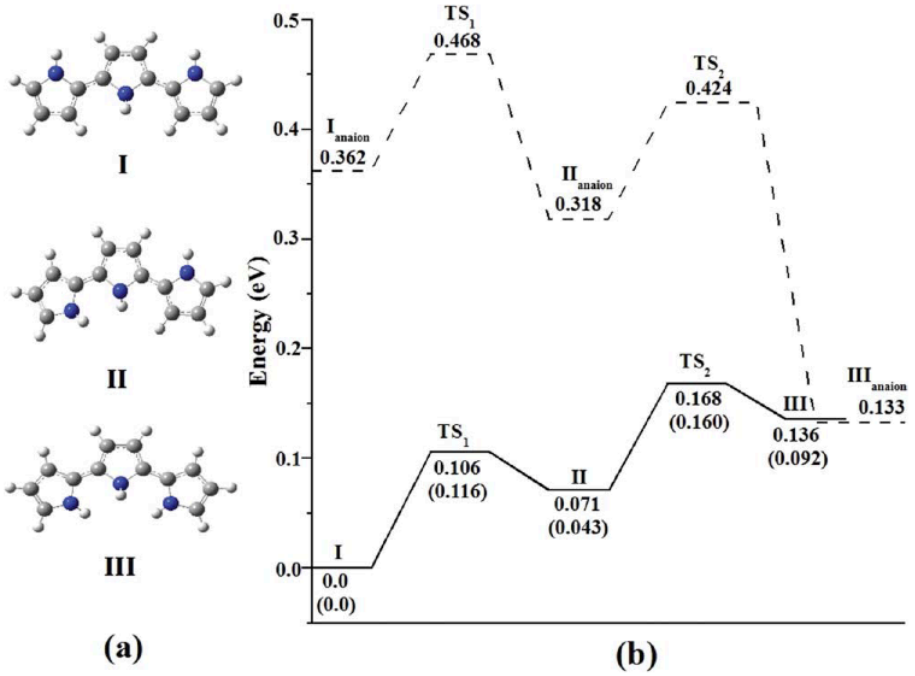

FIGURE 1. Potential energy surface of tripyrrole isomers along the isomerization path calculated within B3PW91/6-311++G. [Color figure can be viewed in the online issue, which is available at wileyonlinelibrary.com.]

electron affinity presumably identifying a dipole-bound anionic state. Values of EAs are reported in Table II. All other anion isomers are less stable than their corresponding neutral isomer as shown in Table I. Two TSs of neutral 4-Py were found to lie at 0.11 eV (0.14 with 6-31+G (3d, 3p)) above the ground state energy of the ↑↓↑↓ isomer to reach the ↑↓↑↑ isomer and 0.24 eV above the ground state (0.29 eV with 6-31+G(3d, 3p)) to reach the ↑↑↑↑ isomer. We predict that to detect experimentally 4-Py$^-$, this oligomer needs first to isomerize, overcoming a barrier of about a quarter eV, and only then an electron would be attachable to the ↑↑↑↑ isomer. This process may occur at very high temperatures.

IR-active vibrational spectra of neutral 2-Py, 3-Py, and 4-Py display two frequency domains, 600–1600 and 3200–3700 cm^{-1}, as shown in Figure 2 (top) for the 6-31+G (3p,3d) case and as was previously reported with the corresponding mode assignments [15]. This spectral distribution is also apparent in the IR-active vibrational spectra of cation oligomers [15]. Most vibrational frequencies in the anion 2-Py$^-$ isomers are comparable to those of the neutral isomers [15, 36], with several modes displaying characteristic red shifts. For example, the N—H stretching mode in the 2-Py *anti-gauche* neutral isomer (C_2) located at 3675 cm^{-1} (intensity of 0.6) is red-shifted to 3557 cm^{-1} in the anion 2-Py$^-$ C_{2h} isomer and becomes the

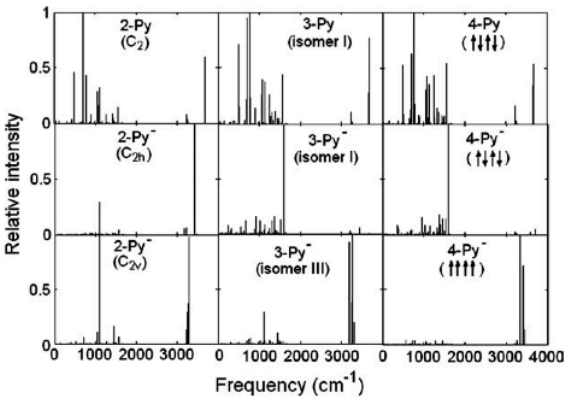

FIGURE 2. IR-active spectra of neutral and anion bipyrrole, tripyrrole, and tetrapyrrole. Spectra on top row correspond to the most stable neutral oligopyrroles. Spectra in the middle row correspond to the anion of the isomers reported at the top. Spectra in the bottom row pertain to the most stable anionic oligopyrroles.

most intense mode of vibration (intensity is 1.0) as illustrated in Figure 2 (middle). Similarly, neutral 2-Py *syn-gauche* isomer (C_{2v}) has its N—H stretching mode located at 3669 cm^{-1} (intensity of 0.16), whereas the mode is red-shifted to 3292 cm^{-1} in the anion 2-Py^- C_{2v} isomer becoming a dominantly intense mode (intensity of 0.97), as shown in Figure 2 (bottom). Another interesting mode in neutral 2-Py *anti-gauche* isomer is the coordinated hydrogen-rocking motion in N—H and C—H bonds. This mode is located at 1126 cm^{-1} with moderate intensity of 0.32 (Fig. 2, top) and is red-shifted to 1099 cm^{-1} (0.29 intensity) in the anion 2-Py^- C_{2h} isomer (Fig. 2, middle). The same hydrogen-rocking mode in neutral 2-Py *syn-gauche* isomer, located at 1131 cm^{-1} (intensity of 0.16), is red-shifted to 1102 cm^{-1} in the anion C_{2v} 2-Py^- isomer becoming the most intense mode of the anion (intensity of 1.0) as seen in Figure 2 (bottom).

Similarly to bipyrrole, both neutral and anion isomers of tripyrrole and tetrapyrrole display IR-active vibrational frequencies in two spectral regions, as shown in Figure 2. IR spectra of the neutral most stable isomers of 3-Py and 4-Py were previously reported in [15] and are depicted in Figure 2 (top). Major differences in the modes of neutral and anion short oligopyrroles are observed for the N—H stretch and the coordinated C=C inter-ring stretch with hydrogen-rocking in C—H and N—H bonds. These two modes in neutral 3-Py isomer I are located at 3676 and 1642 cm^{-1} and have intensities of 0.8 and 0.3, respectively (see Fig. 2 top). Although the C=C stretch at 1594 cm^{-1} in anion 3-Py^- isomer I is the most intense mode (Fig. 2, middle), the dominant mode in anion isomer III (Fig. 2, bottom) at around 3275 cm^{-1} corresponds to N—H stretches in the first and third monomer. Spectra of tetrapyrrole follow a trend similar to tripyrrole. In the neutral 4-Py ↑↓↑↓ isomer (Fig. 2, top), the N—H and C=C stretching modes at 3691 and 1560 cm^{-1} have comparable intensities of 0.5 while a dramatic intensity increase of one of them occurs in the anion isomers. Indeed, the anion ↑↑↑↑ isomer has three intense IR-active lines within 3330–3420 cm^{-1} with relative intensities 1.0, 0.7, and 0.15 that originate from the stretching of the N—H bonds in the two central monomers (Fig. 2, bottom). Correspondingly, the anion ↑↓↑↓ isomer displays its most intense mode around 1600 cm^{-1} corresponding to the C=C stretch plus hydrogen-rockings (Fig. 2, middle). Comparison of neutral 3-Py isomer I and 4-Py↑↓↑↓ isomer IR spectra with calculations in Ref. [36] show differences in relative intensities and no significant differences in frequencies.

Energetics and vibrational results in this section should be important when considering the experimental synthesis of PPy. Indeed, it has been put forward that counterions may induce *anti*-to-*syn* conformation changes along the polymer backbone for producing helical conformations of the polymer chain or their branches [37, 38]. Our results provide concise energies for energy cost-balance and IR spectra signatures, if such conformational changes do indeed occur. The fact that short oligopyrroles have negative electron affinity is indicative that during polymerization in the negatively oxidized phase, short chains and short precursors are not favored.

4. Larger N-Py Anions (n = 6–9, 12, 15, 18) and Effect of Lithium Doping

Full geometry optimization of n-Py is performed for sizes with n = 6, 8, 9 for both neutral and anions with the three basis sets considered. Only neutral and anion n-Py isomers with alternating direction of the N—H bond are analyzed for these larger oligomers because of the high computational cost. For oligomers with n = 12, 15, 18, the geometries of neutral and anion oligomers are fully optimized with the 6-311G basis sets and single point calculations are reported with the 6-311++G and the 6-31+G (3d,3p) basis sets. The reason for this is that comparison of the smaller oligomers optimized structures with the three basis sets shows very small differences in calculated bond lengths and angles, with a consistent decrease in difference as the oligomer length increases. Table III summarizes the binding energies per monomer calculated with this scheme and the three basis sets. Electron affinities of these oligomers are reported in Table II, clearly showing a steady increase with increasing oligomer length. Based on these results, EA increases steadily as a power law: $0.187(n-6)^{1/2}$. However, these electron affinities are very low. To the best of our knowledge, electron affinities of oligopyrroles have not been reported previously in the literature at the level of calculation undertaken in this work.

TABLE III

Binding energy of neutral and anion *n*-Py oligomers.

		Neutral *E*/*n* (eV)				Anion *E*/*n* (eV)		
n	State	6-311G	6-311++G	6-31+G(3d,3p)	State	6-311G	6-311++G	6-31+G (3d,3p)
6	C_2, ^1A	−51.8064	−51.5092	−53.3017	C_1, ^2A	−51.7872	−51.5164	−53.3110
8	C_2, ^1A	−51.6045	−51.3070	−53.0936	C_1, ^2A	−51.6175	−51.3370	−53.1246
9	C_1, ^1A	−51.5375	−51.2397	−53.0244	C_1, ^2A	−51.5576	−51.2740	−53.0595
12	C_2, ^1A	−51.4029	−51.1045	−52.8862	C_1, ^2A	−51.4318	−51.1431	−52.9249
15	C_1, ^1A	−51.3221	−51.0234	−52.8030	C_1, ^2A	−51.3528	−51.0615	−52.8411
18	C_2, ^1A	−51.2684	−50.9694	−52.7474	C_1, ^2A	−51.2995	−51.0054	−52.7835

Binding energies are referred to energies of the isolated atoms (given in Table I caption).

As we have reported in earlier work [15], the geometry of neutral oligopyrroles is strongly bent, and by p-doping with fluorine, the chains become progressively planar as a function of positive increasing oxidation level, acquiring a fully flat structure at a critical value of charge/$n = 1/3$. In contrast, when electrons are injected to the oligopyrroles by electropositive Li-doping, the chain does not become fully flat, even at high uniform doping levels. The charge distribution along the conjugated polymer chain is an important property of charged oligomers. Based on the Mulliken population analysis, with p-doping the positive charge tends to localize over four monomers [15] with a concentration of per monomer to dopant level of 50%. In the oligomer anion the negative charge tends to be pushed to the two end monomers. In doing so, the oligomer becomes more planar as more negative charge is transferred to the molecule from the dopants. Similar to the case of positively charged [15], for multiply charged anionic oligomers, there is a structural change in the conjugated backbone chain from the benzenoid structure (single C_α—$C_{\alpha'}$ bond length between contiguous monomers) to the quinoid structure (double C_α—$C_{\alpha'}$ intermonomer bond length) in chain regions neighboring dopants. Therefore, when electropositve dopants, such as Li atoms are in the proximity of *n*-Py oligomers, a transfer of electrons to the polymer occurs in their immediate proximity. The effect of Li dopants on the alternation of single-double C—C bonds along the conjugated chain of 12-Py is illustrated in Figure 3, where Δl_{C-C} is the change in length of C—C bonds and Δq_C is the change in charge on the C atoms occurring in the doped oligomer with respect to the oligomer without dopants. In Figure 3, α-carbons are depicted with a circle. Calculation for the 6Li-12Py case is based on a full optimization of the geometry of 12-Py with six Li dopants using the 6-311G basis sets. Reported values of energies using the other basis sets correspond to one-point calculation considering that optimized geometry of the doped system. Plots on the left of the figure correspond to the B3PW91/6-31+G (3d, 3p) results, which we compare with our calculation obtained under the HF-M06/6-31+G (3d, 3p) approach depicted on the right. These results correspond to a full optimization of the doped system geometry. It is clear from the figure that irrespective of the method, changes occur preferentially at chain regions where the polymer sustains a negative charge due to electron transfer from dopants in that vicinity. The Li dopants are about 1.9 Å away from the chain, located above and below two contiguous monomers of a four-monomer motif, and the four-monomer motif repeats three times in 12-Py as depicted in the top of Figure 3. This configuration is proved to correspond to a maximum charge transfer of 1.36 e per motif (1.28 e/motif with M06-HF) by inspecting several energy minima of the potential energy surface. We are reluctant to name this anionic 4-Py-motif a "bipolaron" because two full electrons have not been transferred from the two Li dopants to the polymer. Such almost full-electron-transfer has been reported for Li-doped polythiophene [17].

5. Infinite PPy Chain with n-Doping

Neutral PPy is an insulator and when becoming positively charged by p-doping one localized

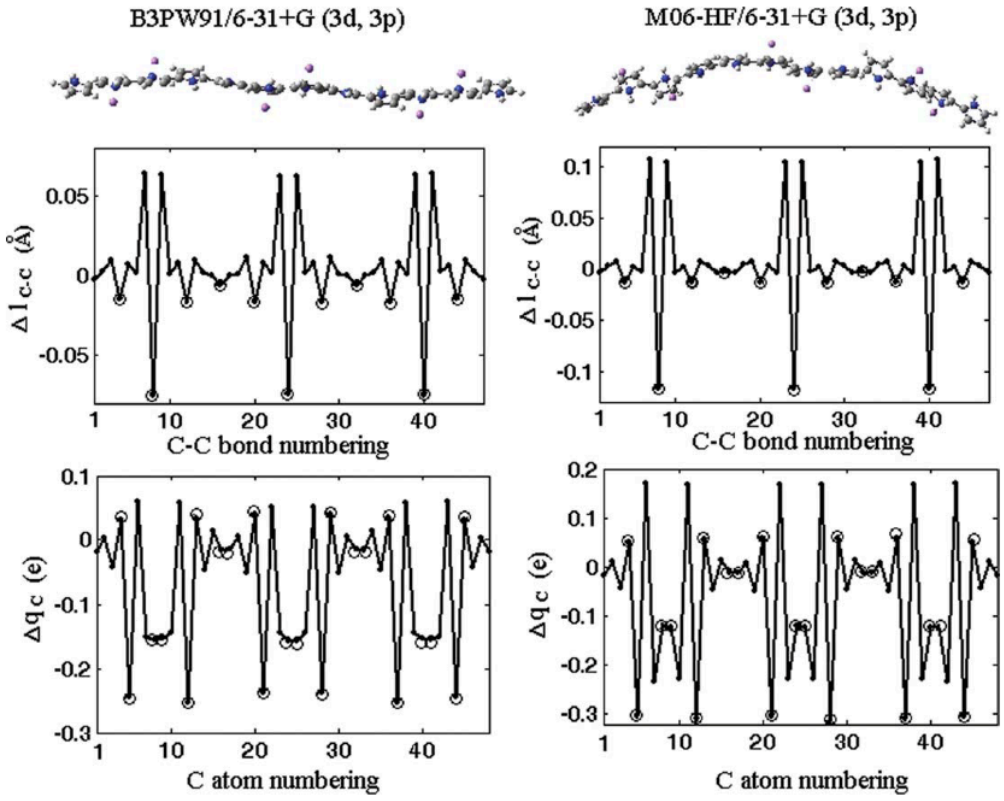

FIGURE 3. Changes of C—C bond length and charge on C atoms along the conjugated chain in 12-Py$^-$ anion with respect to neutral 12-Py. Large circles identify intermonomer locations. [Color figure can be viewed in the online issue, which is available at wileyonlinelibrary.com.]

state appears in the gap per electron removed from the Py ring [15, 16]. In a supplementary recent work [39], we showed that fluorine p-doing of PPy (infinite chain with PBC) introduces two very narrow bands in the gap of pristine neutral PPy at 50% per monomer doping level without significantly reducing the original gap. One of these bands is at 0.5 eV above the Fermi energy E_F and the upper band is about 0.5 eV below the lower unoccupied band. Here, additional calculations within the B3PW91/6-311G approach are performed for the infinite polymer PPy, both pure and n-doped with Li atoms at the same 50% per monomer doping level. Calculations are done with PBC in the X-direction considering a repeatable four-monomer motif in the planar configuration. For this motif, the unit cell length is 14.35 Å. In the case of doped PPy, the unit cell contains the same four-monomer motif plus two Li atoms located one above and one below (at 1.9 Å) two contiguous monomers yielding a 50% per monomer dopant concentration. This positioning of the dopants is the most energetically favorable and results in maximum electron transfer. Figure 4 illustrates a comparison between the one-electron level spectrum of 12-Py and the band structure of PPy. Top plots depict systems without Li dopants whereas the bottom plots show the effect of Li-doping. Energies are referred to the HOMO in the case of 12-Py and E_F in PPy.

In the discrete spectrum of 12-Py, Li dopants give rise to a manifold of states in the proximity of the HOMO located at −3.50 eV. These dopant states are filled, tightly bundled, and placed within the 3.36 eV HOMO–LUMO energy gap of neutral 12-Py. Correspondingly, the band structure of PPy has $E_F = -3.52$ eV and a band gap of 3.2 eV. As illustrated in Figure 4, Li-doped PPy has $E_F = -1.34$ eV, a strongly depleted band gap of 2.4 eV and two dopant narrow bands with widths 0.001 and 0.542 eV located in the gap of pristine PPy. A charge transfer of 1.2 e takes place

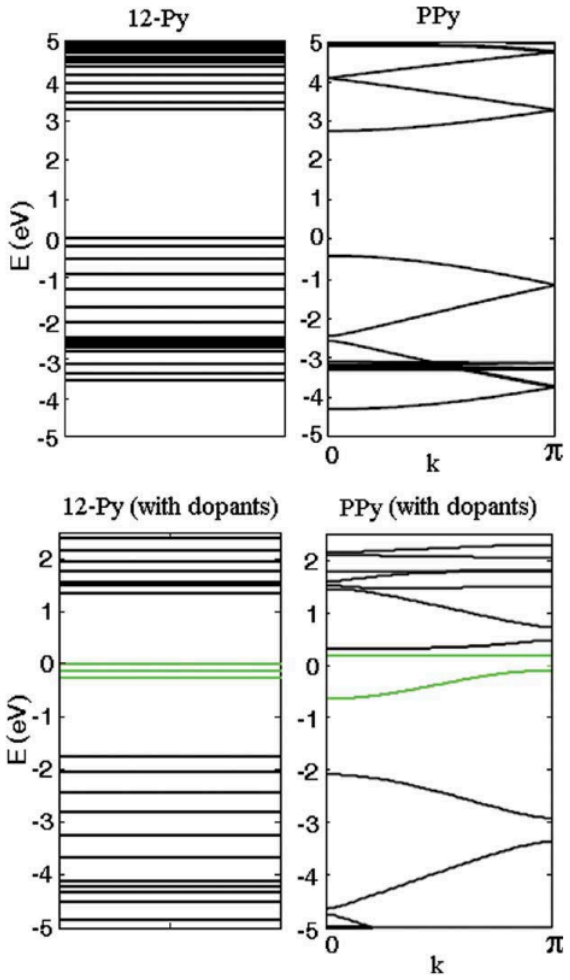

FIGURE 4. Energy spectrum of 12-Py compared with the band structure of PPy for systems without dopants (top) and with Li dopants (bottom). The 12-Py spectrum is obtained with 6-31+G (3d,3p) basis sets and the PPy bands with 6-311G basis sets. [Color figure can be viewed in the online issue, which is available at wileyonlinelibrary.com.]

from the two Li-dopants toward the four-monomer motif in the PPy chain. At $T = 600$ K the total electron occupation of the narrow band below E_F is about 158 with four holes, while the band just above E_F has an electron occupation of about 4. At $T = 300$ K the band below E_F is basically filled (161.7). When compared with our previous results of fluorine p-doped band, it is very noticeable that n-doping reduces the band gap while p-doping doesn't. To be noted in both cases, E_F lies in the gap, and therefore, the doped systems are not metals. A similar behavior is observed for thiophene [17].

Energy of formation of the Li-PPy system may be defined as the difference between the optimized energy of the doped Li-PPy minus the energy of the same PPy configuration without the lithium atoms and plus the energy of two isolated Li atoms. This energy of formation is −0.11 eV, significantly smaller than the oligopyrrole energy of formation of −5.49 eV in 12-Py. This result is consistent with the energetic stabilization of planar chains as the doped system becomes infinite. Worth to note is that in thiophene [17] this energy of formation is positive when calculated at a comparable level of theory.

6. Conclusions

This article reports a thorough study of neutral and anion n-Py oligomers ($n = 2$–18) at the DFT level with large basis sets. The study confirms earlier structure and energetics results within DFT and smaller basis sets for neutral oligomers [15] and puts forward the new structure and energetics results for their anions. Short n-Py oligomers with $n < 6$ attach an electron through dipole-binding. The resulting anions are less stable than their neutral counterparts (negative EA), and thus, may be difficult to detect experimentally. However, larger oligomers have positive EAs that increase with polymer length. These EAs are small as has been speculated in several publications [17, 18]. To the best of our knowledge, EAs of oligopyrroles have not been reported before at our level of calculation.

We demonstrate that in oligomers doped with electropositive Li, the electron transfer mechanism occurs around oligomer monomers in the neighborhood of the dopants. Lithium dopants, at a concentration of 50% per monomer, create an energy-localized bundle of states in the HOMO–LUMO gap of neutral 12-Py. These states are occupied. The corresponding band structure of PPy with Li dopants at the same doping concentration shows the appearance of dopant bands in the energy gap of pristine neutral PPy accompanied by a substantial decrease in the band gap. The decrease in band gap energy is due to the added planarity of the chain produced by the dopants. This effect has been predicted for a variety of other conjugated polymers and their

oligomers [40]. The dopant new bands are narrow and do not cross the Fermi energy. Therefore, the Li-PPy system is not a metal at the doping concentration considered here. Similar results have been reported for Li-doped thiophene even at 100% per monomer doping concentration [17]. In agreement with published results for a variety of other conducting polymers [41], extrapolation of the HOMO–LUMO energy gap in pristine and doped *n*-Py as a function of $1/n$ does not predict the band gap of the infinite chain.

ACKNOWLEDGMENTS

The authors especially acknowledge TeraGrid resources provided by the Pittsburgh Supercomputing Center. Without them this work would have not been possible.

References

1. Dall'Olio, A.; Dascola, G.; Varraca, V.; Bocchi, V. Gazz Chim Ital 1961, 46, 279.
2. Gardini, G. P. Adv Heterocyclic Chem 1973, 15, 67.
3. Chiang, C. K.; Fincher, C. R.; Park, Y. W.; Heeger, A. J.; Shirakawa, H.; Louis, E. J.; Gau, S. C.; MacDiarmid, A. G. Phys Rev Lett 1977, 39, 1098.
4. Li, C.; Bai, H.; Shi, G. Q. Chem Soc Rev 2009, 38, 2397, and references therein.
5. Tran, H. D.; Li, D.; Kaner, R. B. Adv Mater 2009, 21, 1487, and references therein.
6. Garner, B.; Georgevich, A.; Hodgson, A. J.; Liu, L.; Wallace, G. G. J Biomed Mater Res 1999, 44, 121.
7. Lee, J. Y.; Bashur, C.; Goldstein, A.; Schmidt, C. E. Biomaterials 2009, 30, 4325.
8. Ansari, R. Eur J Chem 2006, 3, 186, and references therein.
9. Smela, E. Adv Mater 2003, 15, 481.
10. Smela, E.; Gadegaard, N. Adv Mater 1999, 11, 953.
11. Collier, J. H.; Camp, J. P.; Hudson, T. W.; Schmidt, C. E. J Biomed Mater Res A 2000, 50, 574.
12. Sanghvi, A. B.; Miller K. P.; Belcher, A. M.; Schmidt, C. E. Nat Mater 2005, 4, 496.
13. Fink, J.; Scheerer, B.; Wernet, W.; Monkenbusch, M.; Wegner, G.; Freud, H. -J.; Gonska, H. Phys Rev B 1986, 34, 1101.
14. Okur, S.; Salzer, U. J Phys Chem A 2008, 112, 11842, and references therein.
15. Dai, Y.; Blaisten-Barojas, E. J Chem Phys 2008, 129, 164903.
16. Bredas, J. L.; Themans, B.; Andre, J. M. Phys Rev B 1983, 27, 7827.
17. Ramírez-Solís, A.; Kirtman, B.; Bernal-Jáquez, R.; Zicovich-Wilson, C. M. J Chem Phys 2009, 130, 164904.
18. Colle, R.; Montagnani, R.; Salvetti, O. Theor Chem Acc 1999, 101, 262.
19. Becke, A. D. J Chem Phys 1993, 98, 5648.
20. Frisch, M. J.; Trucks, G. W.; Schlegel, H. B.; Scuseria, G. E.; Robb, M. A.; Cheeseman, J. R.; Scalmani, G.; Barone, V.; Mennucci, B.; Petersson, G. A.; Nakatsuji, H.; Caricato, M.; Li, X.; Hratchian, H. P.; Izmaylov, A. F.; Bloino, J.; Zheng, G.; Sonnenberg, J. L.; Hada, M.; Ehara, M.; Toyota, K.; Fukuda, R.; Hasegawa, J.; Ishida, M.; Nakajima, T.; Honda, Y.; Kitao, O.; Nakai, H.; Vreven, T.; Montgomery, Jr., J. A.; Peralta, J. E.; Ogliaro, F.; Bearpark, M.; Heyd, J. J.; Brothers, E.; Kudin, K. N.; Staroverov, V. N.; Kobayashi, R.; Normand, J.; Raghavachari, K.; Rendell, A.; Burant, J. C.; Iyengar, S. S.; Tomasi, J.; Cossi, M.; Rega, N.; Millam, N. J.; Klene, M.; Knox, J. E.; Cross, J. B.; Bakken, V.; Adamo, C.; Jaramillo, J.; Gomperts, R.; Stratmann, R. E.; Yazyev, O.; Austin, A. J.; Cammi, R.; Pomelli, C.; Ochterski, J. W.; Martin, R. L.; Morokuma, K.; Zakrzewski, V. G.; Voth, G. A.; Salvador, P.; Dannenberg, J. J.; Dapprich, S.; Daniels, A. D.; Farkas, Ö.; Foresman, J. B.; Ortiz, J. V.; Cioslowski, J.; Fox, D. J. Gaussian 09, Revision A.02, Gaussian, Inc.: Wallingford, CT, 2009.
21. Perdew, J. P.; Chevary, J. A.; Vosko, S. H.; Jackson, K. A.; Pederson, M. R.; Singh, D. J.; Fiolhais, C. Phys Rev B 1992, 46, 6671.
22. Perdew, J. P.; Burke, K.; Wang, Y. Phys Rev B 1996, 54, 16533.
23. Lee, C.; Yang, W.; Parr, R. G. Phys Rev B 1988, 37, 785.
24. Stephens, P. J.; Devlin, F. J.; Chabalowski, C. F.; Frisch, M. J. J Phys Chem 1994, 98, 11623.
25. Boese, A. D.; Martin, J. M. L. J Chem Phys 2004, 121, 3405.
26. Zhao, Y.; Truhlar, D. G. J Phys Chem A 2006, 110, 13126.
27. Nygaard, L.; Nielsen, J. T.; Kirchheiner, J.; Maltesen, G.; Rastrup-Andersen, J.; Sorensen, G. O. J Mol Struct 1969, 3, 491.
28. Reed, A. E.; Weinhold, F. J Chem Phys 1983, 78, 4066.
29. Peng, C.; Ayala, P. Y.; Schlegel, H. B.; Frisch, M. J. J Comp Chem 1996, 17, 49.
30. Fukui, K. J Phys Chem 1970, 74, 4161.
31. Gonzalez, C.; Schlegel, H. B. J Chem Phys 1989, 90, 2154.
32. Cances, M.; Mennucci, B.; Tomasi, J. J Chem Phys 1997, 107, 3032.
33. Yurtsever, M.; Yurtsever, E. Syn Metals 1999, 98, 221.
34. Gutowski, M.; Skurski, P.; Boldyrey, A. I.; Simons, J.; Jordan, K. D. Phys Rev A 1906, 1996, 54.
35. Millefiori, S.; Alparone, A. J Chem Soc Faraday Trans 1998, 94, 25.
36. Rabias, I.; Howlin, B. J. Comput Theor Polym Sci 2001, 11, 241.
37. Tamm, T.; Tamm, J.; Karelson, M. Int J Quant Chem 2002, 88, 296.
38. Lin, X.; Li, J.; Smela, E.; Yip, S. Int J Quant Chem 2005, 102, 980.
39. Dai, Y. Doctoral dissertation, George Mason University, 2009.
40. Wijsboom, Y. H.; Patra, A.; Zade, S. S.; Sheynin, Y.; Li, M.; Shimon, L. J. W.; Bendikov, M. Angew Chem Int Ed 2009, 48, 5443.
41. Zade, S; Bendikov, M. Organic Lett 2006, 8, 5243.